SURFACE PROTECTIVE LAYERS OF IRON ALUMINIDES DEVELOPED ON MEDIUM CARBON STEEL BY THE HOT-DIP ALUMINIZING (HDA) PROCESS

Hawkar J. Muhammed
Ph.D. student, University of Miskolc, Institute of Metallurgy
3515 Miskolc, Miskolc-Egyetemváros, e-mail: hawkar@uni-miskolc.hu

Dániel Koncz-Horváth
research fellow, University of Miskolc, Institute of Physical Metallurgy/ Metalforming/ Nanotechnology
3515 Miskolc, Miskolc-Egyetemváros, e-mail: femkhd@uni-miskolc.hu

István Balázs Illés
M.Sc. student, University of Miskolc, Institute of Metallurgy
3515 Miskolc, Miskolc-Egyetemváros, e-mail: metilles@uni-miskolc.hu

Tamás I. Török
professor emeritus, University of Miskolc, Institute of Metallurgy
3515 Miskolc, Miskolc-Egyetemváros, e-mail: fektt@uni-miskolc.hu

Abstract

The investigation in this paper is based on the existence of carbon content and its role in the formation of Fe-Al intermetallic layer in unalloyed carbon steel C45 with a carbon content of 0.44 wt.%. Several sophisticated techniques such as PFIB SEM equipped with EDS and EBSD, GD-OES were employed for the in-depth surface analysis. The results of the metallographic examination reveal that the carbon would appear and could be well detected at the interface between the solidified aluminum and the solid iron-base steel substrate and got also incorporated in the top aluminum layer. Furthermore, due to the dissolution and outward diffusion of iron into the liquid aluminum melt during the HDA process, plus its involvement in the formation of the solid intermetallic surface layer, thus the carbon atoms gaining higher chemical affinity there will also be more likely to form carbide precipitates of different kinds like Fe_3AlC and AlC inside these developing surface layers on the C45 type steel during the process of hot-dip aluminizing at 700 °C.

*Keywords: Hot-dip aluminizing, unalloyed medium carbon steel, carbon content, GD-OES*

1. Introduction

As a protective surface coating, the hot-dip aluminizing (HDA) process has most often been employed on different low-carbon steel substrates (sheets/coils, wires, etc.). The steel carbon content typically ranges between 0.04 and 0.3 wt.%. Unalloyed low-carbon steel sheets, for example, are produced world-wide in several metallurgical plants (clevelandcliffs.com; nipponsteel.com) with a typical aluminum topcoat having thickness ranges between 10 and 20 µm. Below the aluminum topcoat, the thickness range of the bonding interlayer of the iron aluminides is around a few µm. Therefore, such aluminum-

coated steel sheets are recommended to be used and can be utilized without considerable surface degradation, i.e., extensive oxidation/corrosion and/ or discoloration up to about 400 °C in air. However, at much higher temperatures, say, above the melting point of pure aluminum (660 °C), the further evolution and transformation of the iron aluminide interlayers, due to additional high-temperature interdiffusion processes progressing between the top aluminum layer and the substrate iron, are becoming the determining factor. Hence, at higher working or application temperatures, the iron aluminides should be considered primarily as the protective layer (Kobayashi and Yakou, 2002; Deqing, 2008).

Moreover, the formation and evolution features of the iron aluminides so developing, for example, at around 700 °C, do also depend on several technological parameters, like time of immersion, alloying, or contaminating elements of the molten aluminizing bath, and aluminizing temperature were all reported by several researchers (Dey et al., 2020a; Azimaee et al., 2018; Kim, 2013).

In the case of low carbon steels immersed, i.e., hot-dip aluminized, in pure aluminum for different lengths of time, it will show thickening surface inter-layers consisting of growing iron aluminide intermetallic phases, as is illustrated in Figure 1. (Azimaee et al., 2018). The coating thickness growth rate often can be approximated by the well-known parabolic growth rate function (Dey et al., 2020a; Dey et al., 2020b) governed by solid-phase diffusion. However, the actual distribution and orientation of the constituting grains of the intermetallic phase(s) can be rather complex, which is illustrated for the least complicated case of pure iron hot-dip aluminized in high purity molten aluminum at 700 °C for 30 s (Figure 2) (Kishore et al., 2020).
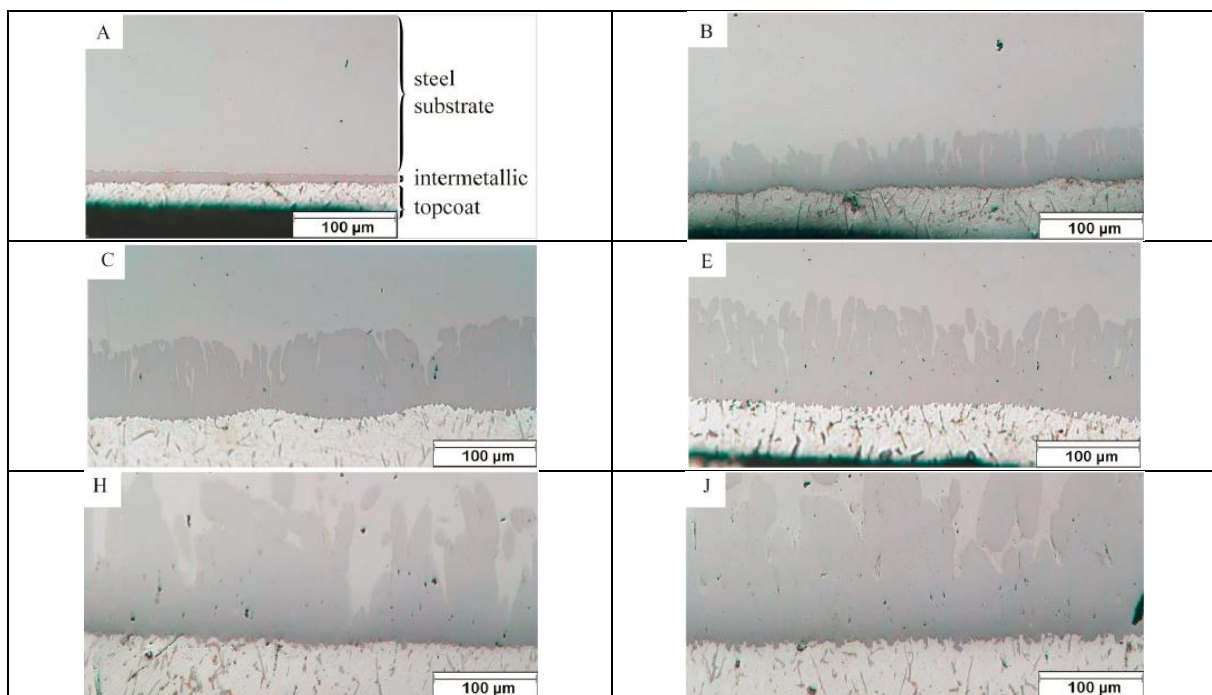
Figure 1. *Effect of immersion time on the thickness and serrated structure of the intermetallic iron aluminide(s) layer formed on low carbon steel hot-dip aluminized at 750 °C. (A) 5 s, (B) 15 s, (c) 30 s, (E) 90 s, (H) 420 s, (J) 900 s (Azimaee et al., 2018).*
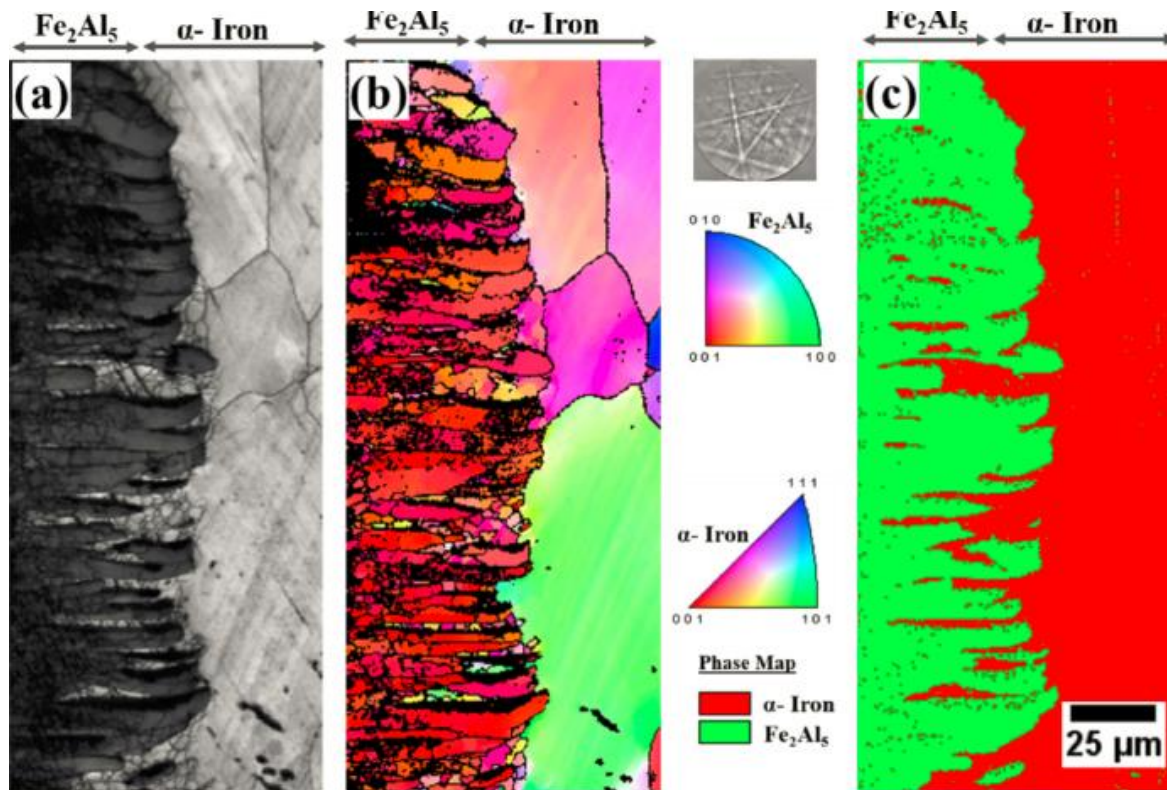
Figure 2. *Typical phases developed on pure iron specimens dipped in molten aluminum (purity > 99.9%) at 700 °C for 30 s (Kishore et al., 2020). Figure 2 part (a) is showing the phase Fe_2Al_5 formed preferentially between the iron substrate and the top aluminum (not shown here on the optical microscopic image). Figure 2 parts (b) and (c) are illustrating the EBSD-orientation /colored inverse pole figure/ and the two major phases (α-Fe and Fe_2Al_5) (Kishore et al., 2020).*

As long as the hot-dip aluminizing process is executed for relatively pure iron base substrates, like unalloyed low carbon steels, and only with pure aluminum containing nothing else but only the common contaminating elements, e.g., iron and silicon at low concentration levels, the chemical and phase composition of the interlayer of the intermetallics will correspond well to those appear in the equilibrium phase diagram of iron and aluminum, i.e., first of all, that of the Fe_2Al_5 grains exhibiting a strong [001] texture along growth direction (Kishore et al., 2020).

However, medium carbon steels as substrates might modify such features of the interlayer due especially to higher amounts of the small size and mobile carbon atoms incorporated in the iron base alloy. The effect of carbon presence in the substrate was studied by others (Niinomi et al, 1982; Hwang et al., 2005; Sasaki et al., 2005) concisely to evaluate its impact on the structure appearance, layer thickness, and the diffusion of iron outward to the molten bath. It was also reported (Niinomi et al., 1982) that the substrate steel's increase in carbon content could cease the iron (Fe) to diffuse out, and silicon and manganese would have the same role.

Therefore, following these aspirations, this research study was done to further explore the major altering effects of carbon on the structure and properties of HDA steel type C45, having an initial total carbon concentration of 0.44 wt.%.

## 2. Materials and experimental method

Commercially pure aluminum was prepared as a molten bath during our laboratory experiments to coat unalloyed medium carbon steel specimens sliced from an extruded rod type C45; afterward, ground polished and degreased. The holding time of the sample inside the molten bath was kept constant at 2.5 minutes, along with the constant temperature during dipping, which was around 695 °C.

2.1. Examination methods

Glow discharge optical emission spectroscopy (GD-OES) GD-profile 2TM from HORIBA was employed to show the distribution profile of the elements developed in the topcoat layer and interdiffusion zone during hot-dipping; in conjunction with the EDS line scanning provided by the PFIB SEM Thermo Scientific Helios G4 apparatus. In addition, structure appearance was carried out via an optical microscope (ZEISS Axioscope) on the sample before and after the HDA process.

3. Results and discussions

The structure of unalloyed carbon steel C45 is depicted in Figure 3. The colony structure of pearlite is shown adjacent to the ferrite structure occupying about 50 percent of the area determined by the Image J software estimation. Thus, this type of steel falls within the hypo-eutectoid region of the iron-carbon phase diagram having an initial structure at room temperature of ferrite and pearlite. Most of the steel's carbon content is present as cementite phase in the perlite grains.
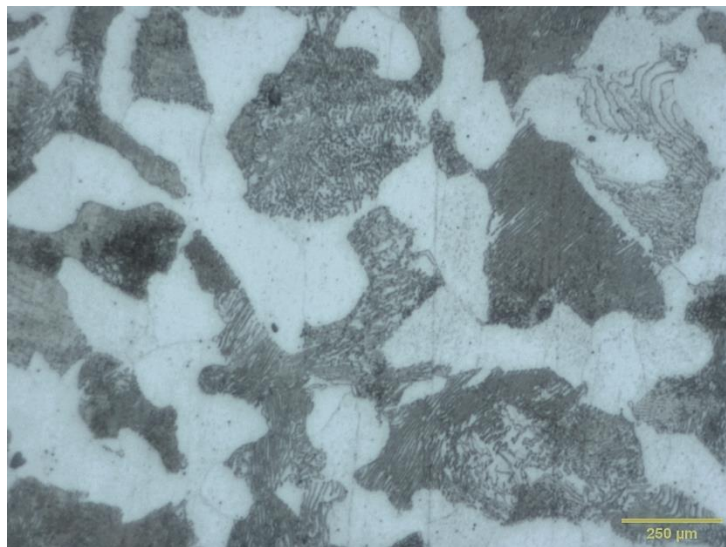
Figure 3. Optical image for unalloyed carbon steel C45 before HDA, the photo was taken perpendicular to the extrusion direction, revealing the distribution of pearlite colonies structure (dark) together with ferrite (white color).

The structure of the hot-dip aluminized carbon steel C45 is shown in Figure 4, wherein the cross-section of the SEM image clearly shows three different layers. The topcoat consists of solidified aluminum followed by the intermetallic layer formed at the interface of solid carbon steel C45 and molten aluminum during the HDA process.
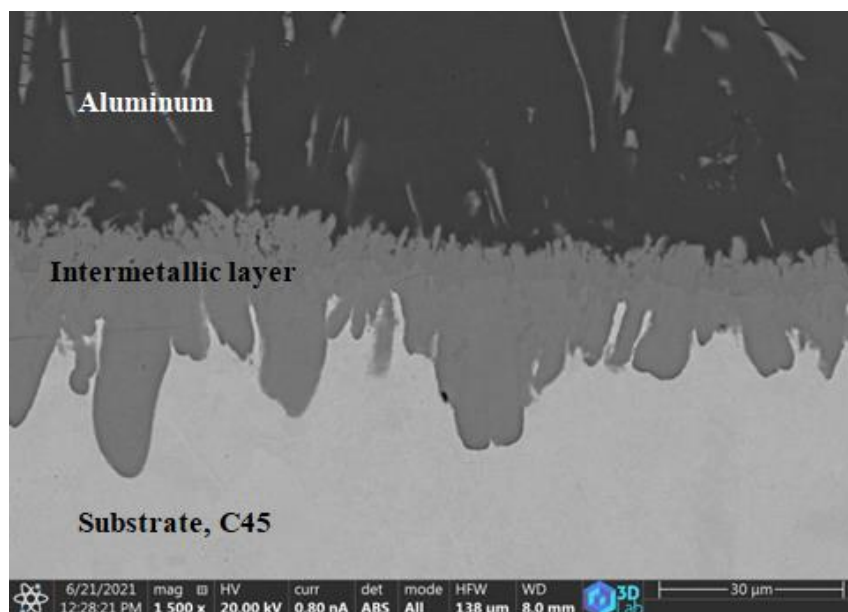
Figure 4. *PFIB-SEM image shows the structure of hot-dip aluminized unalloyed carbon steel C45 when the HDA process temperature was around 695 °C and immersion time was 2.5 minutes inside a molten bath.*

Elemental mapping was carried out to reveal the distribution of elements across the interdiffusion zone and within the topcoat aluminum shown in Figure 5. The elemental mapping for C and Ni could not be recorded with high resolution. However, a few minor spots still appeared in the intermetallic layer being detected together with a few other traces of them in the topcoat aluminum. Therefore, as it is apparent in Figure 5(C),(Ni) for carbon and nickel, respectively, these two elements got also involved in the evolution of the intermetallic structure layer, especially for carbon, due to the substrate high carbon content that could also be seen at the outermost layer where C coexists with Al probably forming aluminum carbide.

As the distribution of the two tested minor elements, i.e., carbon and nickel (See Figure 5 parts (C) and (Ni)), could not be detected with high enough resolution by the applied EDS mapping technique, so the GDOES light spectrometric analytical technique was also employed to try to detect these two minor elements in the surface layers, viz. there is a unique feature of GD OES spectrometry that the elemental in-depth distribution of the constituting chemical elements in principle can be analyzed from hydrogen through carbon to high atomic number ones. Provided that the sample's initial surface is flat and smooth, the GD argon ion sputtering will detach and excite the sample's constituting atoms continuously from a relatively large spot/area of several dozen of mm^2. In this way, the detected intensities for the analyzed elements will present a close-to-average concentration level in the given layer versus sputtering time. In Figure 6, for example, there is a quite pure aluminum top layer sputtered away (i.e., atomized and removed) in about 800 s. While in the sputtering range of ~800 – 1900 s, both major elements of the zone/interlayer of the iron aluminum intermetallics could be well detected, followed by the sputtering of iron (from about 2000 s) inside of the C45 steel substrate. Moreover, the presence of carbon and nickel could also be well detected in the zone of intermetallics (Figure 6.), revealing the result of the outward diffusion of these two alloying elements of the substrate steel during the HDA process.
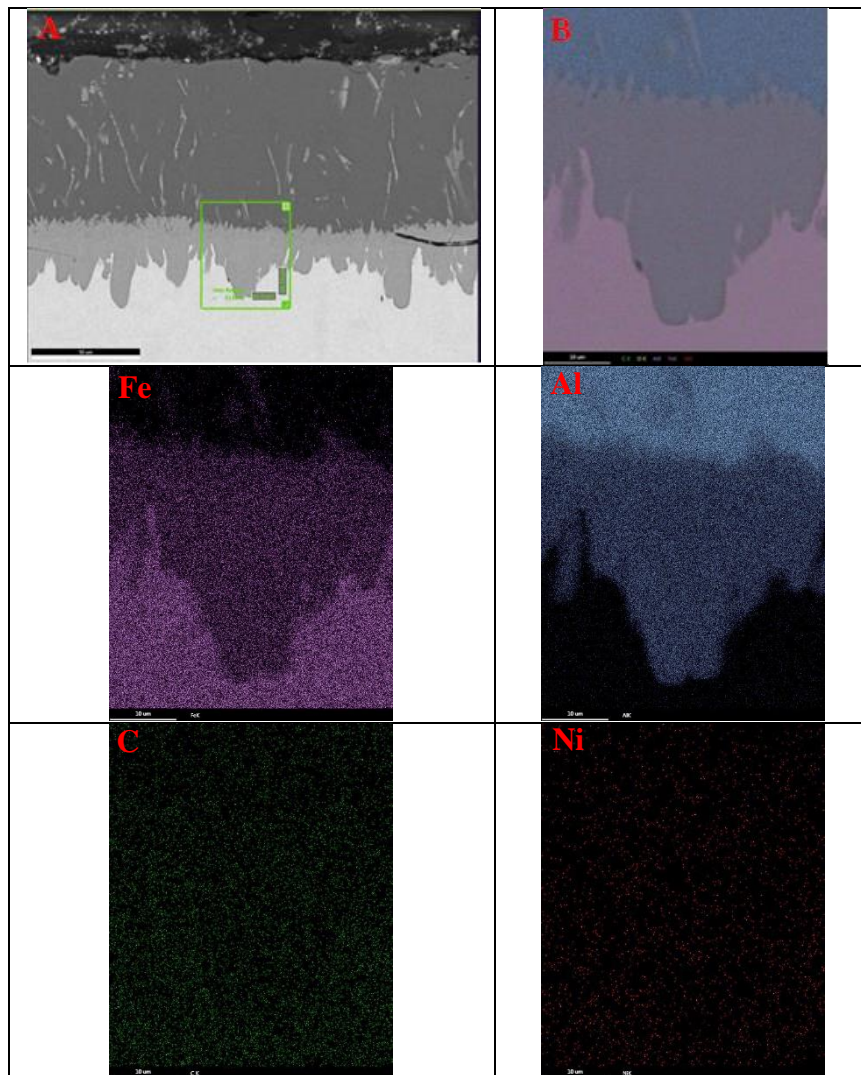
Figure 5. *EDS elemental Mapping for the sectioned HDA sample showing the distribution of the elements within the intermetallic layer and outermost layer, (A) PFIB-SEM image shows the specified area where the elemental mapping was taken, (B) Overlay, (Fe) Fe, (Al) Al, (C) C, (Ni) Ni.*

EDS-line scan was also performed on the cross-sectioned HDA specimen shown in Figure 7. The scan with 0.1 µm steps was taken from the spot just beneath the upper portion of the outermost layer marked on the PFIB-SEM image (Figure 7), where the path of the line scan is also clearly indicated.

The results coincide well with the GD-OES in-depth elemental profiles (Figure 6), where high intensities of the sputtered minor elements carbon and nickel are apparent from about 70 µm in depth from the top. Carbon could also be detected in the Al topcoat layer, most probably forming aluminum carbides such as Al_4C_3 or Fe_3AlC within the interdiffusion zone (Timmerscheidt et al., 2017). The theory behind this phenomenon is attributed to the high chemical affinity of iron (Fe) toward aluminum (Al) (See the

corresponding standard equilibrium thermochemical data in Table 1), which results in the fast formation reaction and evolution of iron aluminides as a newly developing and growing surface layer.


| a) Profile of Fe-Al. | b) *Profile of the two minor elements C and Ni.* |
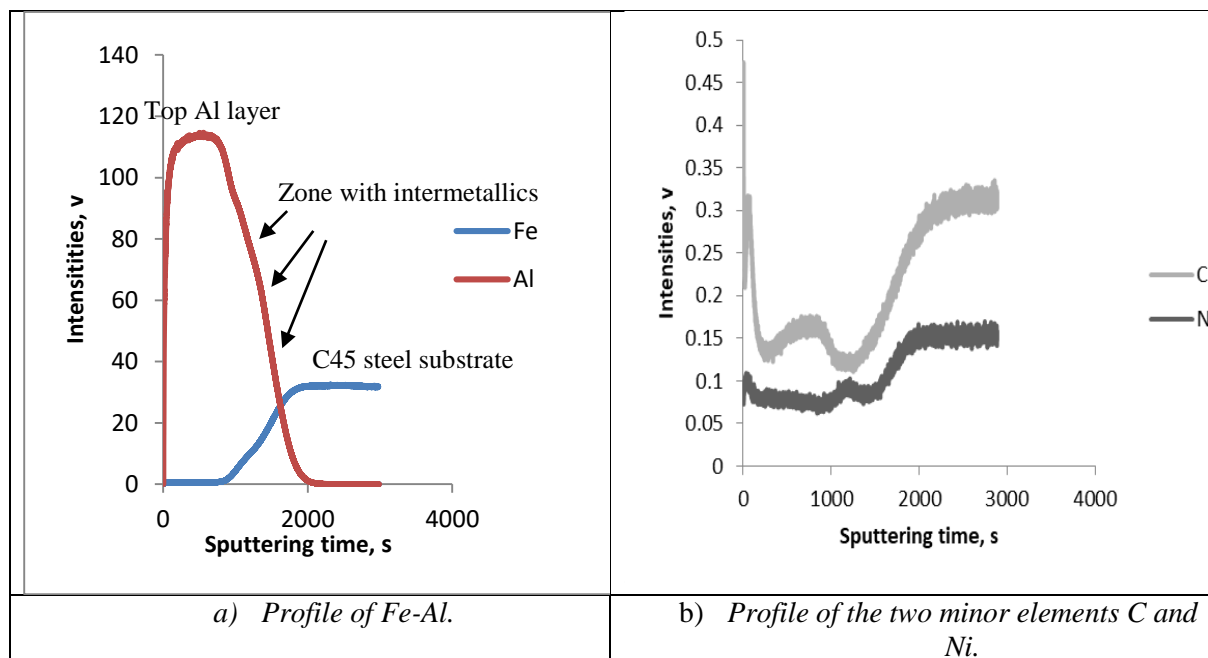
Figure 6. *GD-OES profiles for a) Fe, and Al, together with b) the two minor elements C and Ni vs. the argon-ion sputtering time while forming a crater inwards the sample.*

Both elements have different diffusivity within this solid surface layer, which might cause vacant places within the crystal lattice. As carbon has limited solubility in iron (Fe), it is gaining a higher driving force to diffuse outwards and re-occupy these vacant places (so-called vacancies) within the iron aluminide crystals. The phase analysis results were employed via EBSD to identify the type of carbide formed; the outcomes reveal two types of carbides, Fe_3AlC and AlC, within the intermetallic and topcoat layer Figure 8. In Figure 8(a), a detector analyzed a spot taken from the top portion of the intermetallics layer. The result shows the Fe_3AlC phase formed at the interfaces between the topcoat and intermetallics layers with appropriate CI (confidence index) equal to 0.25 with a significant EBSD pattern. In contrast, in Figure 8(b), where AlC is shown within the topcoat specifically flake-like shape, even the CI is low; however, it owns an acceptable EBSD pattern.

From the thermochemical ΔG values given in Table 1. it can also be deduced that they are also in line with the experimentally observed incorporation of some nickel within the iron aluminide zone Figure 6, due to the exceptionally high negative value for the standard formation Gibbs function of the NiAl phase compared to those of the Fe_xAl_y intermetallics. Thus, the high concentration of carbon in the same zone, at least qualitatively, can be explained by the evolution of new phases of iron aluminides at the interface of steel C45 and aluminum. In this zone, the diffusion of the carbon atoms are not much hindered at the relatively high temperature of the HDA process of this given system.
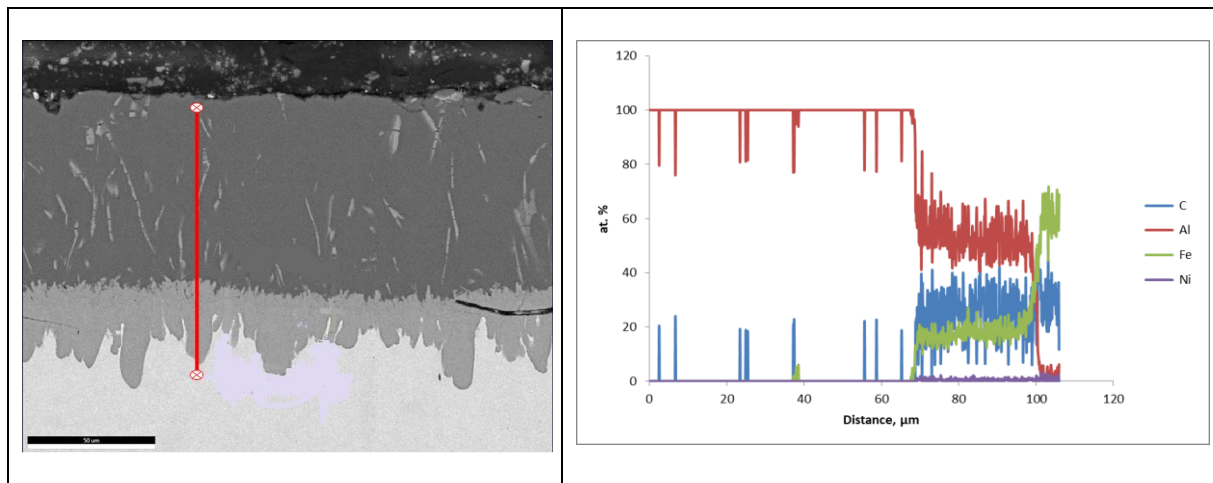
Figure 7. *EDS line scan performed across the cross-section of HDA sample showing also the atomic concentrations of the elements aluminum, iron, carbon, and nickel vs. the measured distance inward down to the substrate steel C45.*
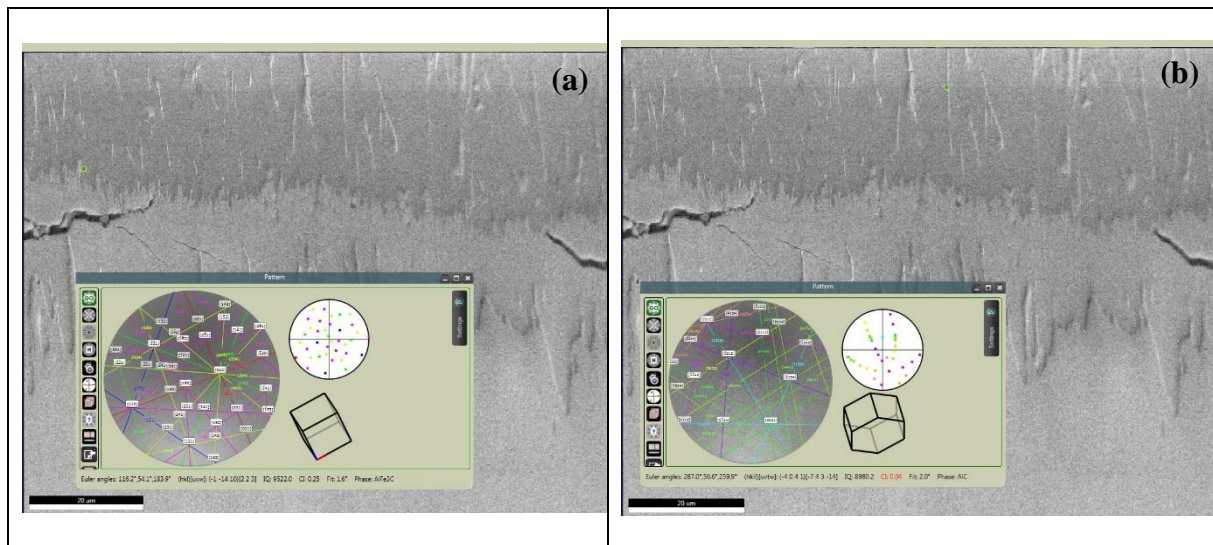
Figure 8. *EBSD spots analysis was examined to specify the type of formed phase during HDA.*

Table 1. *Standard Gibbs free energies of formation for different iron and nickel aluminide compounds calculated at 700 °C using the Software HSC Chemistry version 9.5.1.5 (Outotec HSC Chem.)*

Intermetallic Phases	$\Delta G°$ (kJ/mol)	
FeAl (for1/2 mol)	-49.78 / 2 =	-24.9
$FeAl_2$ (for 1/3 mol)	-77.48 / 3 =	-25.8
$FeAl_3$ (for 1/4 mol)	-110.18 / 4 =	-27.5
Fe_2Al_5 (for 1/7 mol)	-197.58 / 7 =	-28.2
NiAl (for 1/2 mol)	-125.45 / 2 =	-62.7

4. Summary

There are many coupled high-temperature diffusion and chemical compound formation reactions during hot-dip aluminizing of carbon steels. In such a complicated system, in-depth knowledge of the outward diffusion of carbon into the intermetallics layer and its role in forming the iron-aluminum and topcoat layer's grains orientation and distribution is still ambiguous. Therefore, the present study has attempted to specify the distribution/ diffusion of carbon into and within the intermetallics and topcoat layers in more detail.

Several sophisticated experimental techniques were employed to reveal the role of the carbon content of the carbon steel C45 substrate and its influence on the initiation and growth of different intermetallics layers of iron aluminides. The outcomes of all our laboratory tests are consistent with each other and in harmony with the relevant theories and the results of previous studies. During the HDA process, the carbon accumulates at the interface between the liquid aluminum and solid iron. It could also be detected in the topcoat aluminum forming different carbides such as Fe_3AlC and AlC within the intermetallic and topcoat layers. Moreover, these phenomena might become critical when there is a strong requirement to avoid the carbon's presence within the topcoat and/or in the intermetallic layer due to any foreseeable severe corrosion attack when the HDA coated sample is to be exposed to high-temperature environments. Hence, in such harsh environments, the increased tendency of the formation/precipitation of different carbides forming at the interdiffusion zone and topcoat layer might decrease the level of its protective nature.

5. Acknowledgements

References

[1] *Aluminized sheet*. http://www.clevelandcliffs.com/English/Operations/Steelmaking/Indiana-Harbor/default.aspx.

[2] "*aluminized*." https://www.nipponsteel.com/en/.

[3] Kobayashi, S., Yakou, T. (2002). Control of intermetallic compound layers at interface between steel and aluminum by diffusion-treatment. *Mater. Sci. Eng. A*, 338(1-2), 44-53. **https://doi.org/10.1016/S0921-5093(02)00053-9**

[4] Deqing, W. (2008). Phase evolution of an aluminized steel by oxidation treatment. *Appl. Surf. Sci.*, 254(10), 3026-3032. **https://doi.org/10.1016/j.apsusc.2007.10.059**

[5] Dey, P. P., Modak, P., Ghosh, A., Chakrabarti, D., Banerjee, P. S., Ghosh, M. (2020). Investigation of phase evolution of Al–Si–Mg coating on hot dipped interstitial-free steel. *Results Mater.*, 6(February), 100078. **https://doi.org/10.1016/j.rinma.2020.100078**

[6] Azimaee, H., Sarfaraz, M., Mirjalili, M., Aminian, K. (2018). Effect of silicon and manganese on the kinetics and morphology of the intermetallic layer growth during hot-dip aluminizing. *Surf. Coatings Technol.*, 357(October), 483-496. **https://doi.org/10.1016/j.surfcoat.2018.10.035**

[7] Kim, S. K. (2013). Hot-dip aluminizing with silicon and magnesium addition I. Effect on intermertallic layer thickness. *J. Korean Inst. Met. Mater.*, 51(11), 795-799. **https://doi.org/10.3365/KJMM.2013.51.11.795**

[8]   Dey, P. P. et al. (2020). Studies on the characterization and morphological features of the coating on interstitial free steel dipped in molten Al-Si-Mg alloy at 800 ◦C. *J. Mater. Res. Technol.*, 9(3), 4788-4805. **https://doi.org/10.1016/j.jmrt.2020.02.104**

[9]   Kishore, K., Chhangani, S., Prasad, M. J. N. V., Bhanumurthy, K. (2020). Microstructure evolution and hardness of hot dip aluminized coating on pure iron and EUROFER 97 steel: Effect of substrate chemistry and heat treatment. *Surf. Coatings Technol.*, 409(December), 126783. **https://doi.org/10.1016/j.surfcoat.2020.126783**

[10]   Timmerscheidt, T. A. et al. (2017). The role of κ-carbides as hydrogen traps in high-Mn steels. *Metals (Basel).*, 7(7), 1-15. **https://doi.org/10.3390/met7070264**

[11]   Niinomi, M., Ueda, Y., Sano, M. (1982). Dissolution of ferrous alloys into molten aluminium. *Trans. Japan Inst. Met.*, 23(12), 780-787. **https://doi.org/10.2320/matertrans1960.23.780**

[12]   Hwang, S. H., Song, J. H., Kim, Y. S. (2005). Effects of carbon content of carbon steel on its dissolution into a molten aluminum alloy. *Mater. Sci. Eng. A*, 390(1-2), 437-443. **https://doi.org/10.1016/j.msea.2004.08.062**

[13]   Sasaki, T., Yakou, T., Mochiduki, K., Ichinose, K. (2005). Effects of carbon contents in steels on alloy layer growth during hot-dip aluminum coating. *ISIJ Int.*, 45(12), 1887-1892. **https://doi.org/10.2355/isijinternational.45.1887**

[14]   Outotec HSC Chemistry software, version 9.5.1.5, 2020.